Natural Resources Research, Vol. 32, No. 4, August 2023 (© 2023)
https://doi.org/10.1007/s11053-023-10209-0

Original Paper

Effects of Active Hydraulic Fracturing Fluid on the Fracture Propagation and Structural Damage of Coal: Phenomena and Mechanisms

Xiaojie Fang,[1,2] Caifang Wu,[1,2,5] Bin Gao,[1,2] Shasha Zhang,[3] Dan Zhou,[1,2,4] Xiuming Jiang,[1,2] and Ningning Liu[1,2]

Received 22 September 2022; accepted 6 May 2023
Published online: 30 May 2023

Hydraulic fracturing is a common means of reservoir reconstruction in coalbed methane (CBM) wells, but fracturing fluid affects the mechanical properties of weak water-bearing coal seams. To explore the effects of active hydraulic fracturing fluid on coal structural damage, uniaxial compression tests of coal under different fracturing fluid saturations were carried out. Combined with elastic damage mechanics and energy theory, a damage constitutive model of coal under the coupling action of fracturing fluid-stress-strain energy is established, and the rationality and innovation of the model are evaluated. The results show that although micro-cracks have developed in the No. 3 coal seam of the Danshuo Coal Mine, most of them are filled with minerals such as calcite, resulting in poor connectivity between the fractures. The injection of fracturing fluid reduces the cementation strength of the filling body, the bonding force between the coal matrix and the overall mechanical properties of the coal samples. With increase in fracturing fluid saturation and micro-fracture activation, the coal sample brittleness weakens, the compressive strength and elastic modulus decrease linearly, and the shape of the post-peak curve tends to be complex, showing ductile failure characteristics. The principal stress determines the macroscopic fracture direction, the micro-fracture extends along the boundary of calcite–vitrinite and vitrinite–inertinite, and the fracture complexity of inertinite is lower than that of vitrinite. The uniaxial compression damage constitutive model of coal samples containing fracturing fluid based on strain energy and elastic damage mechanics is in good agreement with the experimental data. The model curve is determined by the measured mechanical parameters and the damage constitutive coefficient (n). This can reflect the coal damage constitutive relationship under the coupling action of fracturing fluid-stress-strain energy and is suitable for analyzing the stress-strain problem of coal with fracturing fluid under uniaxial compression.

KEY WORDS: Coal, Fracturing fluid saturation, Uniaxial compression, Strain energy, Damage, Constitutive model.

[1]Key Laboratory of Coalbed Methane Resources and Reservoir Formation Process, Ministry of Education, China University of Mining and Technology, Xuzhou 221008, Jiangsu, China.
[2]School of Resources and Geosciences, China University of Mining and Technology, Xuzhou 221116, Jiangsu, China.
[3]College of Safety Science and Engineering, Henan Polytechnic University, Jiaozuo 454000, Henan, China.
[4]School of Resources and Environment, Henan Polytechnic University, Jiaozuo 454000, Henan, China.
[5]To whom correspondence should be addressed; e-mail: caifangwu@sina.com

INTRODUCTION

Coalbed methane (CBM) is an important supplement to natural gas resources. The development and use of CBM have the triple benefits of supporting economic development, ensuring energy security, and protecting the ecological environment. Most of the CBM reservoirs in China are charac-

terized by complex structure, high degree of metamorphism, strong heterogeneity, low critical desorption pressure and low permeability. These mean that the coal seam needs to be reformed prior to CBM development. Hydraulic fracturing is the most effective and economical method of reservoir reconstruction at present (Wu et al., 2018, 2020; Zhong et al., 2020). The coal seam produces a disturbance effect under the action of hydraulic fracturing, which leads to a change in reservoir structure and mechanical properties from a stable state to an unstable state (Zhao et al., 2019a, 2019b; Hu et al., 2020). In this process, fracturing fluid affects the macroscopic mechanical properties of coal by changing its microstructure, the elastic-plastic state of the reservoir and the evolution of fracture propagation (Tan et al., 2017; Zhao et al., 2018, 2019a, 2019b; Zhang et al., 2020a, 2020b; Cai et al., 2020c). Therefore, it is of great theoretical and practical significance to study the influence of fracturing fluid and stress on the mechanical properties of coal, and this is an important research topic in CBM development engineering.

Physical simulations have been the main means to study the mechanical properties of coal (Vishal et al., 2015; Tan et al., 2017; Lu et al., 2019; Hao et al., 2020), and previous workers have carried out considerable research with the help of various simulation experimental devices (Cai et al., 2020a; Liu et al., 2021; Tao et al., 2021; Xu et al., 2021). On the one hand, the effects of engineering factors such as the loading-unloading path, loading rate and loading mode on the deformation and failure of coal and its mechanical response have been analyzed (Feng et al., 2019; Zong et al., 2020; Xu et al., 2022). On the other hand, the effects of geological factors, such as coal composition, structure, temperature, stress, pressure, gas content and water content, on the mechanical properties of coal have also been studied (Liu et al., 2018; Zhang et al., 2019a, 2019b; Cai et al., 2020c; Li et al., 2020; Wang et al., 2021a, 2021b; Xie et al., 2021; Zhou et al., 2021). The monitoring tools and methods commonly used in the process of physical simulation include acoustic emission, displacement metering, computer tomography scanning, dynamic caustics, digital speckling and electric measurement, based on which abundant fracture mechanical parameters and fracture expansion data have been obtained for coal and rock (Cai et al., 2020b; Song et al., 2020; Zhang et al., 2021a, 2021b). On the basis of physical simulations, previous workers have focused on analyses of mechanical behavior, fracture properties, energy characteristics, damage evolutions, and brittleness evaluations of coal samples under external loads. The proposed coal–rock damage models have been based mostly on statistical data and traditional stress-strain curves, and the degree of regulation of post-peak characteristics has been limited (Borden et al., 2016; Zhang et al., 2020a, 2020b; Zhou et al., 2020; Li et al., 2022). The study of strain energy during compression failure has focused on the laws of energy storage, conversion, release and dissipation, the construction of models for the evaluation of brittleness, and the factors that influence the evolution of energy (Tarasov & Potvin, 2013; Liu et al., 2021; Qiao et al., 2022). Overall, the existing research is beneficial for understanding the mechanical properties and deformation and failure laws of coal reservoirs (Sampath et al., 2018; Liu et al., 2020; Lu et al., 2020). However, research on the cooperative control of fracture expansion, matrix deformation, energy evolution and damage of coal samples by fracturing fluid is insufficient at present, and the existing damage models cannot reflect the control effect of fracturing fluid saturation (w), stress, and strain energy on the failure process of coal.

In view of this, based on the physical simulation experiment of uniaxial compression, combined with elastic damage mechanics and energy theory, the deformation and failure process and energy evolution of coal samples with different fracturing fluid saturations during uniaxial compression were analyzed in this study. A damage constitutive model of coal samples with fracturing fluid in the whole process of uniaxial compression was constructed, and the rationality and accuracy of the constitutive model were verified by the measured data. These research results can provide a theoretical basis for the hydraulic fracturing of CBM wells.

MATERIALS AND METHODS

Basic Parameters of Coal in the Study Area

The experimental samples were collected from the No. 3 coal seam of the Danshuo Coal Mine in the Laochang mining area of eastern Yunnan, with average burial depth of 410 m (Zhang et al., 2021a, 2021b). Coal blocks with complete structures and sizes larger than 200 mm were selected from the working face of the Danshuo Mine, numbered and wrapped in plastic wrap, black plastic bags, trans-

Table 1. Test results of coal quality and density

Sample ID	Proximate analysis (%)				Apparent density (g/cm^3)	True density (g/cm^3)
	M_{ad}	A_d	V_{daf}	FC_d		
DS-4	1.71	14.59	10.23	76.67	1.38	1.43
DS-6	1.79	13.60	10.57	77.26	1.42	1.48
DS-3	1.75	14.94	9.72	76.80	1.34	1.40

M_{ad} , moisture content; A_d , dry base ash; V_{daf} , dry ash free basis volatile; FC_d , fixed carbon content

Table 2. Test results of coal petrography

Sample ID	Nonmineral (%)		Contain mineral (%)					$R_{o,max}$ (%)
	Vitrinite	Inertinite	Organic	Clay	Sulfides	Carbonate	Silicon dioxide	
DS-4	91.55	8.45	96.24	0.63	–	2.50	0.63	3.14
DS-6	80.93	19.07	96.20	1.27	–	2.53	–	3.13
DS-3	85.71	14.29	83.65	3.77	–	8.18	4.40	3.28

parent glue and foam paper in turn, packed in a packing box with a buffer bubble cushion and transported back to the laboratory.

The coal quality characteristics and test results of the true and apparent densities of the experimental coal samples are shown in Table 1. The coal sample of the Danshuo Coal Mine is low and medium ash anthracite with average apparent density of 1.38 g/cm^3 and true density of 1.44 g/cm^3. The coal petrography test results are shown in Table 2. The macrolithotype of the coal was semi-dull to semi-bright, the average content of vitrinite was 86.06%, inertinite was 13.94%, and exinite was not detected. The inorganic minerals were mainly carbonates, followed by clay and silica.

The microscopic images of coal samples from the Danshuo Mine under the scanning electron microscope are shown in Figures 1 and 2. The coal matrix was dense, the cross section was diverse, and most of the pores were irregular (Fig. 1a and b). The microfractures in the coal matrix were well developed, the widths of the fractures were mostly between several hundred nanometers and a few microns, the surfaces of the fractures were smooth and extended far away, and most of them were shear cracks (Fig. 1c). In addition, the bedding plane and most of the cracks in the coal seam were filled with, among others, calcite and clay minerals. The filling area was banded and densely reticulated, resulting in poor connectivity between cracks (Fig. 1d). The reason for the above phenomena is that the coal seam underwent different stages and intensities of tectonics in the sedimentary process, which led to pore deformation, and secondary fractures were generally developed and filled by minerals.

Sample Preparation

According to the suggestion of ISRM, the sample preparation process of uniaxial compression tests (UCTs) with different fracturing fluid saturations is as follows. (1) Cylindrical samples with diameter (D) of 50 mm and height (H) of 100 mm were drilled along the parallel bedding direction, and the samples were carefully polished so that the nonuniform error was controlled below 0.05 mm and the non-parallelism of the two ends was less than 0.1 mm. (2) The polished coal samples were placed in a drying box and dried at 70 °C for 24 h. After that, the samples were removed and weighed every 3 h until the quality of the coal samples no longer changed. It was then assumed that the movable moisture in the coal samples was completely lost, and the dry weight of the samples was recorded. (3) An active hydraulic fracturing fluid with 2% KCl concentration was prepared with KCl powder and distilled water. The dried coal samples were placed in a vacuum pressure saturation device under vacuum for 6 h, saturated with fracturing fluid for 18 h, and weighed. The saturated weight of the coal samples was recorded, and the saturated liquid

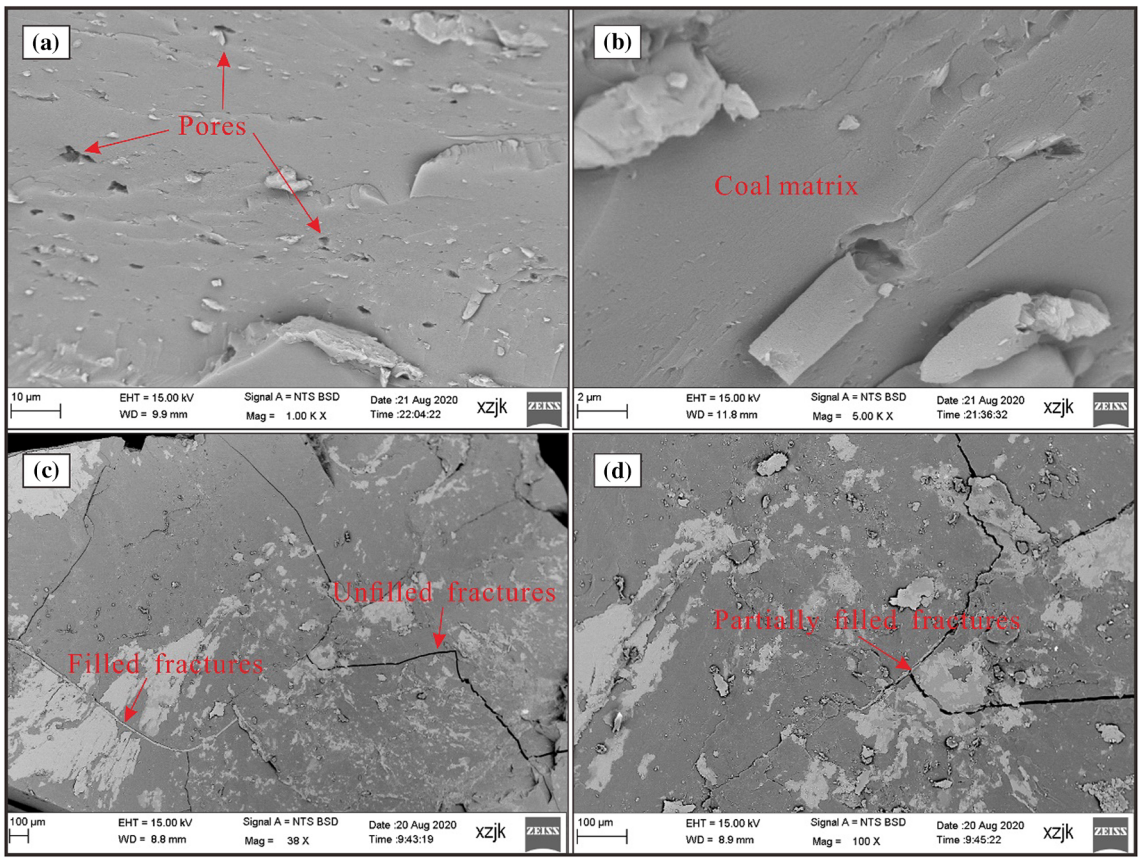

Figure 1. SEM images of the coal samples from the Danshuo Mine.

content of the coal samples was calculated. (4) Taking the fracturing fluid saturations of 0, 25, 50, 75 and 100% as variables, the quality of each sample was calculated when it reached theoretical saturation; the coal samples were placed indoors so that the fracturing fluid could evaporate naturally until the coal sample quality reached the theoretical value, and then the coal samples were wrapped with cling film to complete the sample preparation. The basic information on coal samples with different fracturing fluid saturations is shown in Table 3.

It should be noted that the DS5-2, DS5-3 and DS2-1 samples with 0% saturation of fracturing fluid were not subjected to vacuum pressure saturation treatment as the control group of coal samples after fracturing fluid treatment. Except for the above three coal samples, the mass of other coal samples after drying ranged between 276.62 and 308.77 g, with average of 287.79 g. The mass of fully saturated coal samples ranged between 280.13 and 311.83 g, with average of 291.86 g. The amount of fracturing fluid absorbed by different coal samples in the saturation process ranged from 2.23 to 8.07 g, with average of 4.07 g. There were differences in the quality of different coal samples and the amount of fracturing fluid absorbed during saturation, which is related to the material composition, porosity, fracture development degree, mineral content and properties of coal. Almost all the fluid produced by the existing CBM wells in the study area was fracturing fluid (Qin et al., 2018; Yang et al., 2020). The results show that the water content of the No. 3 coal seam was weak and that it was a typical weak water-bearing coal seam. The mechanical properties of coal were mainly affected by the in situ stress regime of the reservoir and fracturing fluid in the fracturing process.

Testing System and Procedures

Uniaxial compression deformation tests of coal samples with different fracturing fluid saturations were carried out using the TAW-2000 microcom-

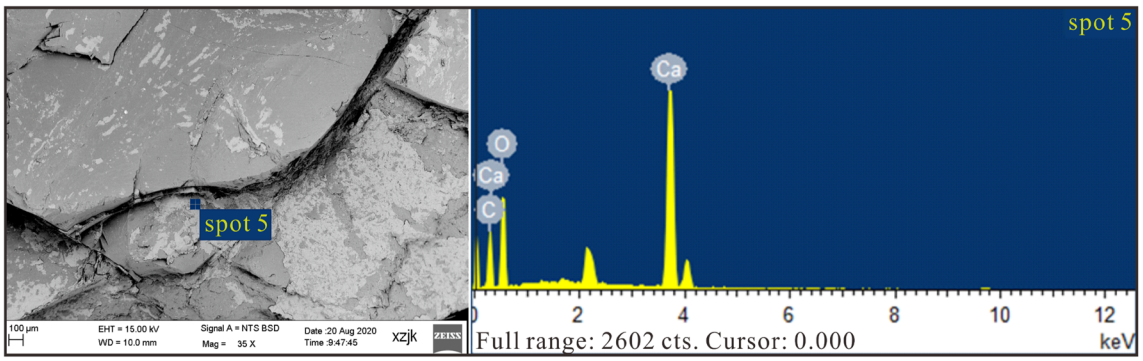

Figure 2. Morphology and EDX spectrum analysis of calcite.

Table 3. Basic information of coal samples with different fracturing fluid saturations

Saturation (%)	Sample ID	H (mm)	D (mm)	Dry weight (g)	Saturated weight (g)	Liquid mass (g)	Theoretical quality (g)
0	DS5-2	100.15	49.94	285.49	–	–	285.49
	DS5-3	100.17	49.95	286.24	–	–	286.24
	DS2-1	100.10	50.04	314.95	–	–	314.95
25	DS1-3	100.16	50.11	294.90	298.65	3.75	295.84
	DS4-1	100.42	49.95	290.82	293.49	2.67	291.49
	DS4-2	100.25	49.91	291.51	293.74	2.23	292.07
50	DS1-2	100.40	50.10	281.17	285.68	4.51	283.43
	DS5-4	100.30	49.92	288.00	293.99	5.99	291.00
	DS4-3	100.41	49.91	285.00	288.41	3.41	286.71
75	DS5-5	100.18	49.98	290.48	295.00	4.52	293.87
	DS5-1	100.28	50.02	288.72	291.35	2.63	290.69
	DS5-6	100.28	49.94	308.77	311.83	3.06	311.07
100	DS1-1	100.44	49.95	280.56	285.01	4.45	285.01
	DS4-4	100.61	49.89	276.62	280.03	3.51	280.13
	DS3-1	100.32	49.93	276.95	285.12	8.07	285.02

puter-controlled electrohydraulic servo rock triaxial testing system. The testing system was mainly composed of a control system, pump, loading machine, and strain measuring device. The device is shown in Figure 3. The stiffness of the host of the loading machine was greater than 10 GN/m, the loading capacity was 2000 kN, the upper limit of confining pressure was 100 MPa, and the minimum time interval of computer data acquisition was 1 ms.

After the coal samples with different fracturing fluid saturations were prepared, they were placed between the upper and lower heads of the loading machine, the loading machine was started, and axial compression was applied at a speed of 0.001 mm/s until the coal sample was completely unstable. During the experiment, an ASM linear displacement transducer was used to measure the axial and radial strain of the coal samples, and the computer-controlled program was used to record the axial stress (σ_1), axial strain (ε_1) and radial strain (ε_3) during the whole process.

TEST RESULTS AND DISCUSSION

Uniaxial Mechanical Properties

Figure 4 shows the changes in uniaxial compressive strength (σ_c), peak strain (ε_c), elastic modulus (E) and Poisson's ratio (υ) with fracturing fluid saturation. Compared with dry coal samples, the strength damage of coal samples with 25, 50, 75 and 100% fracturing fluid saturation can reach 3.37, 37.81, 15.18 and 72.30%, respectively (Fig. 4a). The damage of E can reach − 1.15, 32.99, 19.47 and 59.91%, respectively (Fig. 4c). It is known that the

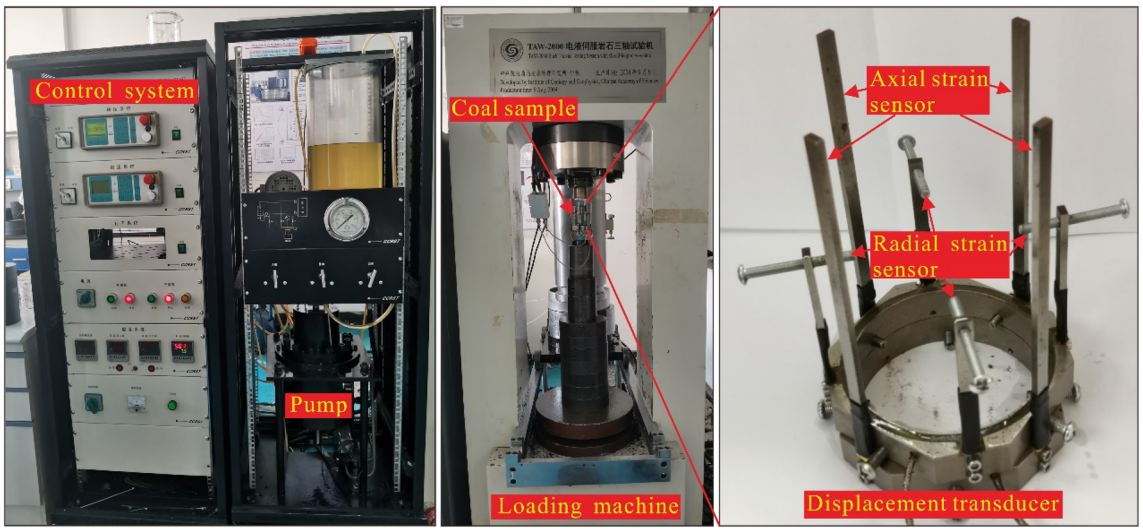

Figure 3. Compression experimental system for coal samples.

mechanical properties of coal samples show a weakening trend under the influence of fracturing fluid, especially when the mechanical properties of fully saturated coal samples decrease greatly, which is consistent with previous studies on the effect of multiphase fluid saturation on the mechanical properties of coal and rock (Zhang et al., 2019a, 2019b; Lai et al., 2020). The ε_c of coal samples with different fracturing fluid saturations does not show obvious regularity but fluctuates within the range of 0.35–0.52 mm (Fig. 4b), indicating that fracturing fluid mainly affects the mechanical bearing capacity of coal, and the ε_c of coal samples is mainly controlled by the material composition of the coal matrix itself. In addition, the relationship between υ and fracturing fluid saturation is not obvious. However, the coal samples taken from the same coal block DS5 still show a certain regularity; the υ of dry coal samples is 0.21, and υ reaches 0.37 and 0.33 when the fracturing fluid saturation increases to 50 and 75%, respectively (Fig. 4d), indicating that when other factors remain the same, υ increases with increasing fracturing fluid saturation. The main reason why the υ of different coal samples does not show obvious regularity is that the deformation characteristics of different coal blocks are different, that is, coal has strong anisotropy. By comparing the changes in different mechanical parameters with the fracturing fluid saturation, it is found that σ_c and E are more affected by the fracturing fluid, ε_c is controlled by the coal matrix itself, and υ has stronger anisotropy.

The stress-strain curves of coal samples with different fracturing fluid saturations are shown in Figure 5. Combined with the basic parameters of the coal samples in Table 3, it was found that the increase in fracturing fluid saturation led to the weakening of brittleness, the shape of the curve tended to be complex, the failure process tended to be relaxed, and the mechanical properties showed an obvious weakening phenomenon. Compared with dry coal samples, the proportion of the stress-strain curve in the post-peak stage increased with increasing fracturing fluid saturation, indicating that the energy stored in the compaction, elasticity and yield stage of dry coal samples was released rapidly in the post-peak stage, which led to the instability and failure of coal samples, while the coal samples with higher fracturing fluid saturation slowly released energy in the post-peak stage, and the failure of coal samples showed ductile characteristics.

Failure Characteristics

The morphology of coal samples with different fracturing fluid saturations showed the following characteristics: (1) the fracture complexity increased with increasing fracturing fluid saturation, the surface of the high-saturation coal sample broke and

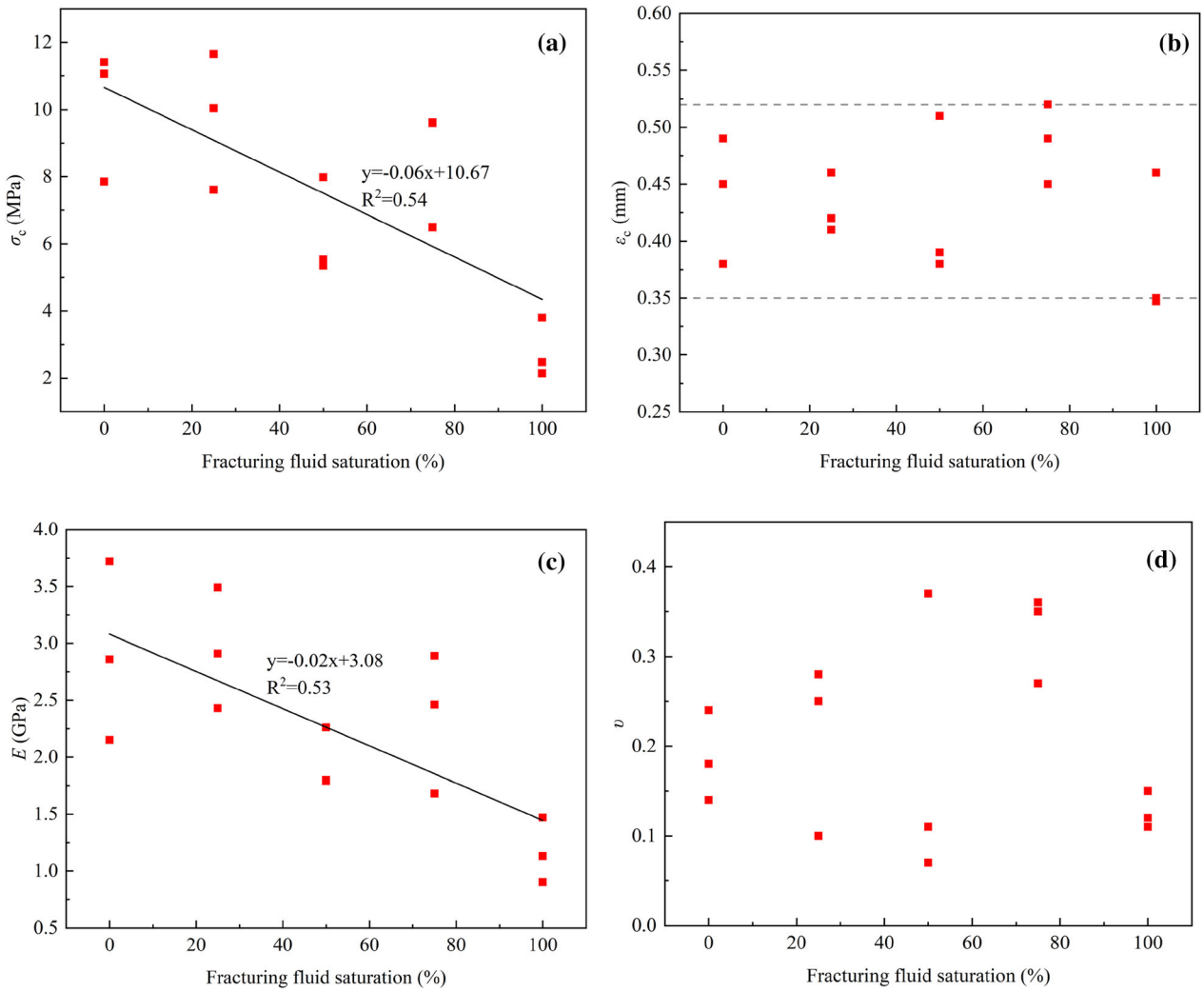

Figure 4. Comparisons of σ_c, ε_c, E and υ of the coal samples.

collapsed, and water marks were seen on the fracture surface, indicating that the lubrication of fracturing fluid promoted the destruction of coal samples. (2) The low-saturation coal samples exhibited mainly shear failure and axial splitting, and obvious penetrating cracks were seen on the surface of the coal samples after failure, but the scale and number of radial cracks were small. A large number of non-penetrating fractures were developed along the radial direction of high-saturation coal samples that were orthogonal or oblique to the axial penetrating cracks, which greatly increased the complexity of the failure morphology of coal samples (Fig. 6). The above characteristics are due to two aspects. One is that the carbonate and clay minerals filled in micro-fractures softened, became muddy and dissolved under the action of water in the fracturing fluid, and the adhesion between the coal matrix decreased, which led to fracture activation and reduced the difficulty of relative slip of the fracture surface. On the other hand, the pores and cracks of coal were closed gradually under the action of fracturing fluid and external load, and the fracturing fluid that could not be discharged in time increased the pore water pressure in the coal, which promoted the concentration of tensile stress at the tip of the natural fracture and led to fracture expansion. These findings are consistent with those in previous quasistatic experimental studies of the weakening effect of water on rock strength (Wong

et al., 2016; Cai et al., 2019; Zhong et al., 2019). Corresponding to the stress-strain curve, the failure degree of the coal samples increased with increasing fracturing fluid saturation, indicating that the coal samples of high-pressure fracturing fluid saturation broke gradually and that the fracture expanded fully in the process of slow elastic release.

To further analyze the distribution characteristics and failure mode of coal microfractures, the fracture morphology of coal before and after compression was observed and recorded by electron microscopy (Fig. 7). The development of natural fractures in dry coal samples was high, but most of the microfractures were filled by minerals, and the connectivity between them was poor (Fig. 7a), which is consistent with the test results of coal in section Basic Parameters of Coal in the Study Area. The micro-fractures in dry coal samples expanded mainly along the boundary between calcite and vitrinite, and the micro-fractures terminated at the boundary between inertinite and vitrinite. Combined with previous research results (Hol et al., 2012; Pan et al., 2013; Zhao et al., 2019a, 2019b; Puskarczyk et al., 2022), the brittleness of vitrinite is considered stronger than that of inertinite (Fig. 7b). The coal samples with 50% fracturing fluid saturation formed chiefly main fractures parallel to the loading direction along the boundary between vitrinite and inertinite. The shape of the main fractures was relatively straight, and some of them were orthogonal to the main fractures. However, the calcite veins of the activated filled fractures had not been dissolved largely (Fig.7c). The coal samples with 100% saturation of fracturing fluid formed a main fracture parallel to the loading direction along the boundary of vitrinite and inertinite and between vitrinite and the calcite vein. The increase in fracturing fluid saturation reduced the intensity of vein cementation and activated the filling fracture, which was orthogonal to the main fracture, making the shape of the fracture more complex (Fig.7d and e).

Based on the macro- and micro-fracture morphology of coal samples and the changes in the physical and chemical properties of coal, combined

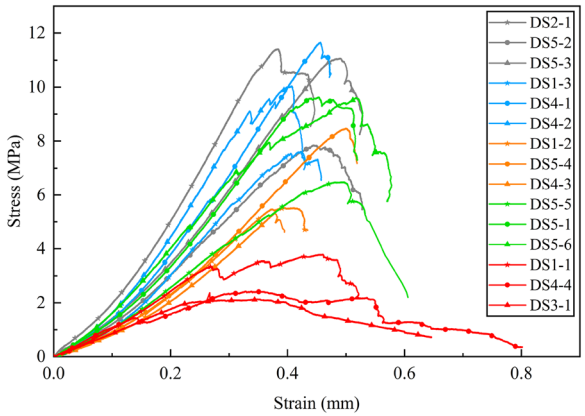

Figure 5. Uniaxial stress–strain curves of the coal samples with different water saturations.

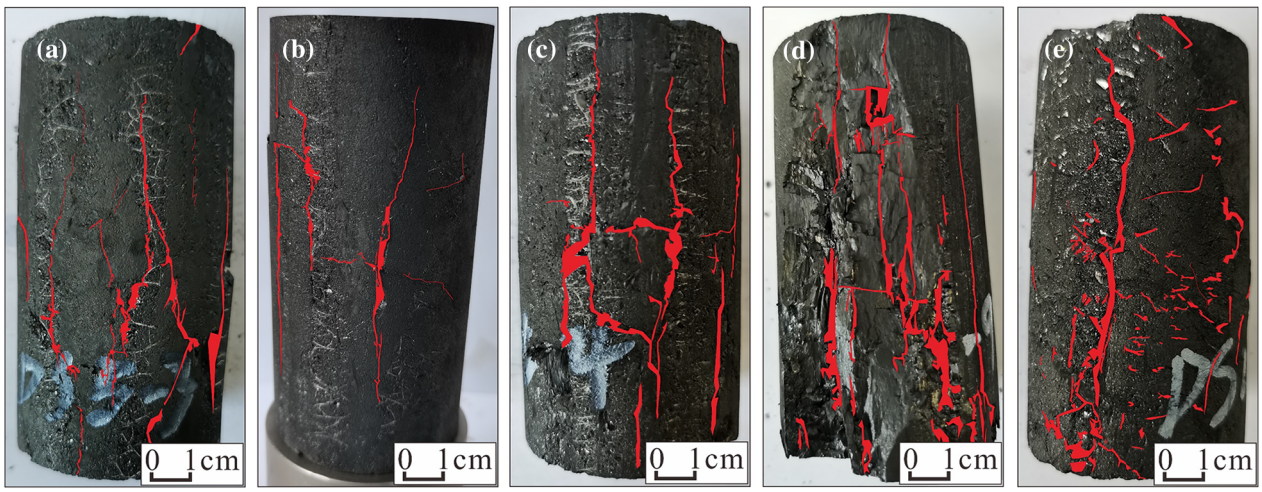

Figure 6. Uniaxial compression failure mode of coal samples with different fracturing fluid saturations (**a**) 0%: DS5-3; (**b**) 25%: DS4-2; (**c**) 50%: DS5-4; (**d**) 75%: DS5-6; (**e**) 100%: DS3-1.

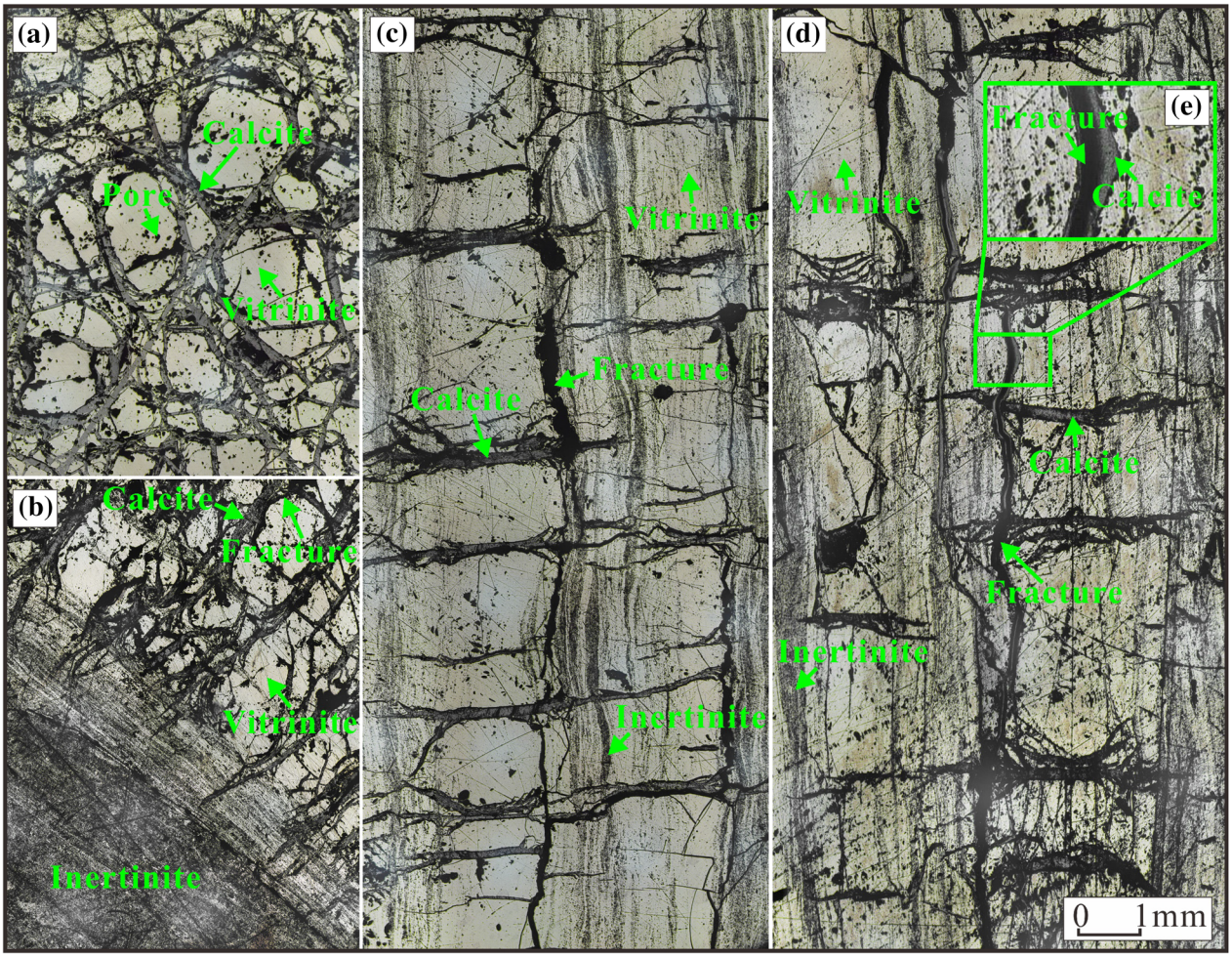

Figure 7. Distribution characteristics of micro-cracks in coal samples under uniaxial compression: (**a**) calcite vein filling fracture; (**b**) fractures terminate at inertinite; (**c**) 50% saturation of fracturing fluid; (**d**) 100% saturation of fracturing fluid; (**e**) partial magnification of Figure 7d.

with the research results of Yao et al. (2021), it is considered that the coal samples containing fracturing fluid were controlled by tension and shear at the same time under an external load, and the effect of fracturing fluid on the friction coefficient between fracture surfaces was less than that on particle cementation, which is the main reason for the transition from shear failure in the dry state to tension–shear composite failure in the saturated state.

Energy Evolution and Structural Damage

Energy Parameters

The deformation and failure of coal samples during loading is an energy-driven instability phenomenon (Wen et al., 2020; Yin et al., 2021). According to the law of conservation of energy, without considering the external heat exchange, it can be considered that the total energy (U) of coal samples in the compression process is composed of elastic energy (U^e) and dissipated energy (U^d) (Fig. 8). The expression is (Liu et al., 2016):

$$U = U^e + U^d \tag{1}$$

For the triaxial compression process, U and U^e can be characterized by the stress and strain of coal samples, which are calculated, respectively, as:

$$U = \int_0^{\varepsilon_1} \sigma_1 d\varepsilon_1 + 2\int_0^{\varepsilon_3} \sigma_3 d\varepsilon_3 \tag{2}$$

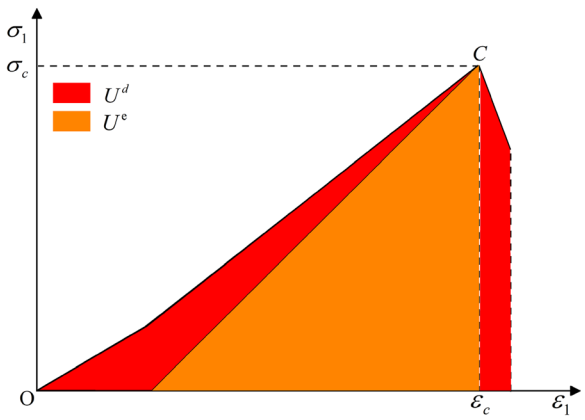

Figure 8. Characteristics of the energy distribution during uniaxial compression.

$$U^e = \frac{1}{2}\sigma_1\varepsilon_1^e + \sigma_3\varepsilon_3^e \tag{3}$$

where σ_3 is radial stress, $\varepsilon_1{}^e$ is axial elastic strain and $\varepsilon_3{}^e$ is radial elastic strain. According to Hooke's law, combined with the research results of Xie et al. (2011) and Wang et al. (2021a, 2021b), Eq. 3 can be rewritten as:

$$U^e = \frac{1}{2E_u}[\sigma_1^2 + 2\sigma_3^2 - 2\upsilon(2\sigma_1\sigma_3 + \sigma_3^2)] \tag{4}$$

where *Eu* is the unloading modulus. For the uniaxial compression process, $\sigma_3 = 0$, $E_u \approx E$, and Eqs. 2 and 4 can be rewritten as:

$$U = \int_0^{\varepsilon_1} \sigma_1 d\varepsilon_1 \tag{5}$$

$$U^e = \frac{1}{2E}\sigma_1^2 \tag{6}$$

By substituting Eqs. 5 and 6 into Eq. 1, the expression of dissipated energy in the process of uniaxial compression is obtained, thus:

$$U^d = \int_0^{\varepsilon_1} \sigma_1 d\varepsilon_1 - \frac{1}{2E}\sigma_1^2 \tag{7}$$

In addition, σ_c and ε_c in Figure 8 are the uniaxial compressive strength and peak strain, respectively, where the peak strain is the axial strain when the coal sample reached σ_c.

Construction of the Fracturing Fluid-Stress-Strain Energy Damage Model

The failure process of coal under uniaxial compression is controlled essentially by the accumulation and dissipation of energy, but existing damage models fail to take into account the effect of energy on coal damage. Therefore, considering the effect of the above energy parameters in the construction of the damage model, this study explored the construction of a damage model governed by the fracturing fluid, stress, and strain energy.

For weak water-bearing coal seams, a large amount of active hydraulic fracturing fluid injection in a short time will have an important impact on the mechanical properties of the coal seam, mainly manifested in the deterioration of mechanical properties, damage to the coal structure and a rapid evolution of reservoir energy. At the initial stage of applying stress, the strain energy was concentrated mainly at the tip of the natural fracture. As the stress increased, the coal samples released energy in the form of plastic failure during crack development. According to the theory of macroscopic damage mechanics and the first law of thermodynamics, the damage degree was characterized by the difference in energy characteristics of coal samples with different fracturing fluid saturations, and it was assumed that the damage of coal samples with 0% fracturing fluid saturations was 0. The fluid damage variable of the coal sample under the influence of fracturing fluid was defined by the change in elastic energy under different fracturing fluid saturations, thus:

$$D_w = 1 - \frac{U_w^e}{U_0^e} \tag{8}$$

where D_w is the damage variable when the fracturing fluid saturation is w, $U^e{}_0$ is the elastic energy when the fracturing fluid saturation is 0%, and $U^e{}_w$ is the elastic energy when the fracturing fluid saturation is w. Equation 6 was inserted into Eq. 8 to obtain:

$$D_w = 1 - \frac{E_0\sigma_{1w}^2}{E_w\sigma_{10}^2} \tag{9}$$

where E_0 is the E when the fracturing fluid saturation (MPa) was 0%, σ_{10} is the axial stress when the fracturing fluid saturation (MPa) was 0%, E_w is the E when the saturation (MPa) of the fracturing fluid

was w, and σ_{1w} is the axial stress when the fracturing fluid saturation (MPa) was w.

The damage of the microelement under an external load was random and difficult to characterize by a single eigenvalue. Assuming that there was no obvious plastic deformation in the pre-peak stage of uniaxial compression, the damage deterioration degree of the meso-microelement can be described by the forced damage variable (D_ε), which is expressed as (Zhu & Tang, 2004; Li et al., 2021):

$$D_\varepsilon = \begin{cases} 0 & \varepsilon_1 < \varepsilon_c \\ 1 - (\varepsilon_c/\varepsilon_1)^n & \varepsilon_1 \geq \varepsilon_c \end{cases} \tag{10}$$

where n is the damage constitutive coefficient. According to Lemaitre's strain-equivalent principle, combined with the stress condition of uniaxial compression, the following relations can be obtained (Lemaitre, 1992):

$$[\sigma^*] = \frac{[\sigma_1]}{[1 - D_\varepsilon]} = \frac{[C][\varepsilon_1]}{(1 - D_\varepsilon)} \tag{11}$$

where $[\sigma^*]$ is the effective stress tensor, $[\sigma_1]$ is the nominal stress tensor, $[C]$ is the elastic modulus tensor and $[\varepsilon_1]$ is the strain tensor. It was assumed that the mechanical properties of coal are macroscopically isotropic, that the elastic phase dominates before uniaxial compression failed, and that the stress-strain relation of coal was consistent with Hooke's law. The constitutive relation for mechanical damage in coal is:

$$\sigma_1 = E(1 - D_\varepsilon)\varepsilon_1 \tag{12}$$

Considering that the total energy before the peak was composed of elastic energy and dissipated energy, the elastic coefficient (u) was defined as:

$$u = \frac{U^e}{U^e + U^d} \tag{13}$$

Considering the effects of coal mechanical properties, fracturing fluid and axial load on coal damage, according to Eqs. 9 and 13, the following relationship can be obtained:

$$E = uE_w = \frac{uE_0\sigma_{1w}^2}{(1 - D_w)\sigma_{10}^2} \tag{14}$$

By substituting Eq. 14 into Eq. 12, the damage characteristics of coal under the coupling action of fracturing fluid-stress-strain energy can be obtained, thus:

$$\sigma_1 = \frac{uE_0\sigma_{1w}^2}{(1 - D_w)\sigma_{10}^2}(1 - D_\varepsilon)\varepsilon_1 \tag{15}$$

Combining Eqs. 10 and 15, the damage constitutive model of coal samples containing fracturing fluid in the whole process of uniaxial compression can be expressed by the piecewise function:

$$\sigma_1 = \begin{cases} \frac{uE_0\sigma_{1w}^2}{(1-D_w)\sigma_{10}^2}\varepsilon_1 & \varepsilon_1 < \varepsilon_c \\ \frac{uE_0\sigma_{1w}^2}{(1-D_w)\sigma_{10}^2}\frac{\varepsilon_c^n}{\varepsilon_1^{n-1}} & \varepsilon_1 \geq \varepsilon_c \end{cases} \tag{16}$$

Model Verification and Parameter Discussion

To verify the rationality and accuracy of the whole process damage constitutive model of coal samples with fracturing fluid under uniaxial compression based on strain energy and elastic damage mechanics, the damage parameters of coal samples with different fracturing fluid saturations were counted and calculated, and these parameters were substituted into Eq. 15. The model curves were drawn in turn and compared with the actual curves of the UCTs of each coal sample. The parameters of the damage model of coal samples containing fracturing fluid are shown in Table 4.

The comparison of the stress-strain experimental curves and model curves of coal samples with different fracturing fluid saturations is shown in Figure 9. The results showed that the constitutive model constructed in this study reflected well the strength characteristics of coal and rock under the action of fracturing fluid and axial stress. The damage constitutive model curve was similar to the experimental results in the pre-peak and post-peak stages, and the theoretical curve was in good agreement with the measured data. Coal is close to an elastic brittle body in the process of uniaxial compression, and the axial strain increased linearly

Table 4. Parameters in the coal damage constitutive model with different fracturing fluid saturations

Samples	w (%)	ε_c	E (MPa)	u	n
DS5-3	0	0.49	2993	0.76	4
DS4-2	25	0.41	3484	0.72	8
DS5-4	50	0.50	2257	0.74	5
DS5-5	75	0.50	1705	0.78	4
DS3-1	100	0.35	905	0.76	4

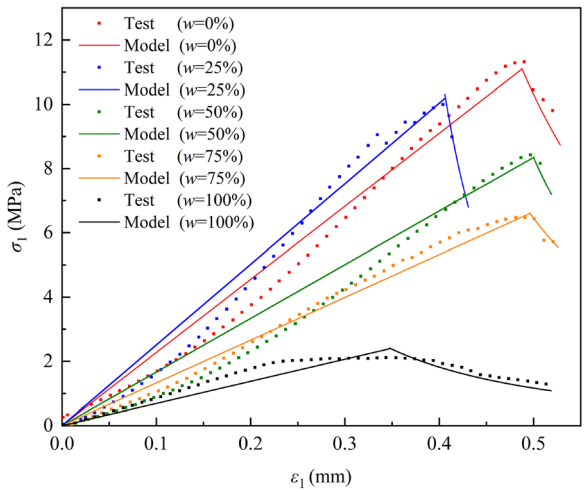

Figure 9. Comparison between the test and theoretical curves in the coal damage constitutive model.

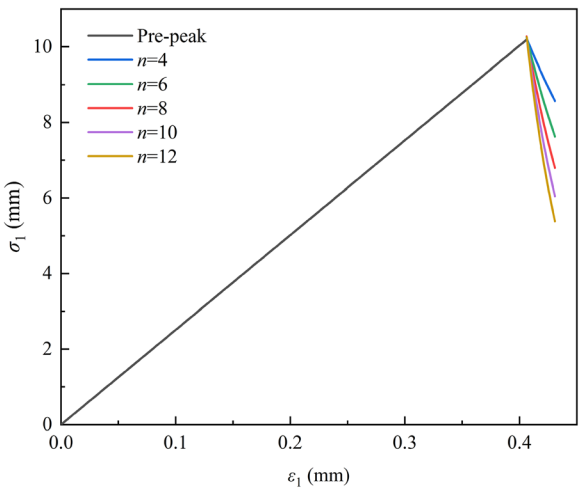

Figure 10. Effect of parameter n on the theoretical deviatoric stress-strain curve.

with increasing axial stress in the pre-peak stage. Both the theoretical curve and the experimental curve decreased linearly in the post-peak stage, and the slope of the post-peak curve of coal samples with saturation below 75% was larger than that in the pre-peak stage, indicating that the internal damage of coal developed continuously in the post-peak stage, and the strain energy absorbed in the pre-peak stage was released rapidly after the coal sample reaches uniaxial compressive strength.

The theoretical values of σ_c and ε_c calculated by the theoretical model were consistent with the experimental results, the post-peak bearing capacity was lost, and there was no residual strength, which further reflects the rationality of the theoretical model. Overall, the theoretical model constructed in this study can reflect the deformation and strength characteristics of coal in the whole process of uniaxial compression, and the accuracy of the model was better than that of the traditional continuous statistical damage constitutive relation.

On the basis of model verification, the influence of model parameters on the shape of the theoretical curve was discussed, and the rationality of model parameters was further analyzed. The pre-peak characteristics of the theoretical curve were controlled by E, axial stress, axial strain and u, and the related parameters can be calculated from the experimental results. The post-peak characteristics of the model depended on E, axial stress, axial strain, u, and n. Except for n, the other parameters came from the experimental results. Using coal sample DS4-2 as an example, the influence of n on the theoretical curve was analyzed when the other parameters remained constant. The results are shown in Figure 10. It can be seen that n affects the magnitude of the M-Descendant modulus, which is shown in the control of the speed and degree of stress drop. In summary, the damage constitutive model established in this study was determined by the measured mechanical parameters and n of coal.

It should be noted that there was some deviation between the constitutive model built based on the basic assumptions of elasticity and the measured data in this study, which is mainly reflected in that the gradient of the measured values in the compaction stage and yield stage of uniaxial compression was smaller than the calculated results of the model, which reflects the plastic enhancement of coal in these two stages. The reason lies in the compaction of the micro-pores and fractures in the compaction stage and the activation of the fracturing fluid on the micro-cracks in the yield stage. Therefore, to develop a more appropriate energy constitutive model for the uniaxial compression process in coal, it was necessary to modify the destruction variables in the compaction and yield stages. Related content is a difficulty that has received extensive attention from researchers in this field and will continue to be studied in depth in follow-up work.

CONCLUSIONS

(1) The complexity of fractures in weak water-bearing coal strata under the influence of multistage tectonic movements is affected by active hydraulic fracturing fluid. For a coal seam in the Danshuo Coal Mine in eastern Yunnan, micro-cracks are developed in the coal matrix, but most of them are filled with calcite and other minerals, which lead to the deterioration of the connectivity between the fractures. The injection of fracturing fluid reduces the cementation strength of the filling body and the adhesion between the coal matrix and complicates the fracture shape.

(2) The mechanical properties of coal samples show a weakening trend under the influence of fracturing fluid. Compared with dry coal samples, the σ_c damage of fracturing fluid-saturated coal samples was 72.30%, and the E damage was 59.91%, both of which were linearly related to saturation. With the increase in fracturing fluid saturation, the brittleness of the coal sample weakens, the fracture expands fully, and the shape of the post-peak curve tends to be complex, showing ductile failure characteristics.

(3) Fracture propagation is affected by macerals, main stress direction and fracturing fluid saturation. The main stress determines the macroscopic fracture direction, and the microfracture extends along the boundary of calcite vein–vitrinite and vitrinite–inertinite and terminates at the inertinite-vitrinite boundary. The increase in fracturing fluid saturation promotes the dissolution of calcite and other minerals in filling fractures, which is the main cause of fracture activation.

(4) The uniaxial compression damage constitutive model of coal samples containing fracturing fluid based on strain energy and elastic damage mechanics is in good agreement with the experimental data. The model curve is determined by the measured mechanical parameters and parameter n, which can reflect the damage constitutive relation of coal under the coupling action of fracturing fluid–stress–strain energy and is suitable for analyzing the stress-strain problem of coal with fracturing fluid under uniaxial compression.

FUNDING

This work was supported by the National Natural Science Foundation of China (41872170, 42130802), a Project Funded by the Priority Academic Program Development of Jiangsu Higher Education Institutions, Qian Science Cooperation Project of Prospecting Strategy ([2022]ZD001–001, [2022]ZD001–003), Key Laboratory of Coalbed Methane Resources and Reservoir Formation Process of the Ministry of Education (China University of Mining and Technology) (No. 2022–009), the Fundamental Research Funds for the Central Universities (2023XSCX002), the Graduate Innovation Program of China University of Mining and Technology (2023WLKXJ002), and the Postgraduate Research & Practice Innovation Program of Jiangsu Province.

DATA AVAILABILITY

All data generated or analyzed during this study are included in this published article.

DECLARATIONS

Conflict of Interest The authors declare that they have no known competing financial interests or personal relationships that could have appeared to influence the work reported in this paper.

REFERENCES

Borden, M. J., Hughes, T. J. R., Landis, C. M., Anvari, A., & Lee, I. J. (2016). A phase-field formulation for fracture in ductile materials: Finite deformation balance law derivation, plastic degradation, and stress triaxiality effects. *Computer Methods in Applied Mechanics and Engineering, 312*, 130–166.

Cai, X., Zhou, Z., Liu, K., Du, X., & Zang, H. (2019). Water-weakening effects on the mechanical behavior of different rock types: Phenomena and mechanisms. *Applied Sciences, 9*, 4450.

Cai, X., Zhou, Z., Tan, L., Zang, H., & Song, Z. (2020a). Fracture behavior and damage mechanisms of sandstone subjected to wetting-drying cycles. *Engineering Fracture Mechanics, 234*, 107109.

Cai, X., Zhou, Z., Tan, L., Zang, H., & Song, Z. (2020b). Water Saturation effects on thermal infrared radiation features of rock materials during deformation and fracturing. *Rock Mechanics and Rock Engineering, 53*, 4839–4856.

Cai, X., Zhou, Z., Zang, H., & Song, Z. (2020c). Water saturation effects on dynamic behavior and microstructure damage of sandstone: Phenomena and mechanisms. *Engineering Geology, 276*, 105760.

Feng, P., Dai, F., Liu, Y., Xu, N. W., & Du, H. B. (2019). Coupled effects of static-dynamic strain rates on the mechanical and fracturing behaviors of rock-like specimens containing two unparallel fissures. *Engineering Fracture Mechanics, 207*, 237–253.

Hao, D., Tu, S., Zhang, C., & Tu, H. (2020). Quantitative characterization and three-dimensional reconstruction of bituminous coal fracture development under rock mechanics testing. *Fuel, 267*, 117280.

Hol, S., Spiers, C. J., & Peach, C. J. (2012). Microfracturing of coal due to interaction with CO_2 under unconfined conditions. *Fuel, 97*, 569–584.

Hu, Q., Liu, L., Li, Q., Wu, Y., Wang, X., Jiang, Z., Yan, F., Xu, Y., & Wu, X. (2020). Experimental investigation on crack competitive extension during hydraulic fracturing in coal measures strata. *Fuel, 265*, 117003.

Lai, X., Zhang, S., Cui, F., Wang, Z., Xu, H., & Fang, X. (2020). Energy release law during the damage evolution of water-bearing coal and rock and pick-up of AE signals of key pregnancy disasters. *Chinese Journal of Rock Mechanics and Engineering, 39*, 433–444.

Lemaitre, J. (1992). *A course on damage mechanics*. Springer-Verlag.

Li, B., Wang, Z., Ren, C., Zhang, Y., Xu, J., & Li, J. (2021). Mechanical properties and damage constitutive model of coal under the coupled hydro-mechanical effect. *Rock and Soil Mechanics, 42*, 315–323.

Li, J., Li, B., Pan, Z., Wang, Z., Yang, K., Ren, C., & Xu, J. (2020). Coal permeability evolution under different water-bearing conditions. *Natural Resources Research, 29*, 2451–2465.

Li, T., Gao, M., Chen, G., Meng, L., Zhang, Y., & Yin, H. (2022). A method for evaluating brittleness of hard rocks based on thermal-mechanical damage constitutive parameters. *Chinese Journal of Rock Mechanics and Engineering, 41*, 2593–2602.

Liu, X., Hao, Q., Hu, A., & Zheng, Y. (2020). Study on determination of uniaxial characteristic stress of coal rock under quasi-static strain rate. *Chinese Journal of Rock Mechanics and Engineering, 39*, 2038–2046.

Liu, X., Ning, J., Tan, Y., & Gu, Q. (2016). Damage constitutive model based on energy dissipation for intact rock subjected to cyclic loading. *International Journal of Rock Mechanics and Mining Sciences, 85*, 27–32.

Liu, X., Zhang, Z., Ge, Z., Zhong, C., & Liu, L. (2021). Brittleness evaluation of saturated coal based on energy method from stress-strain curves of uniaxial compression. *Rock Mechanics and Rock Engineering, 54*, 3193–3207.

Liu, Y., Tang, D., Xu, H., Li, S., & Tao, S. (2018). The impact of coal macrolithotype on hydraulic fracture initiation and propagation in coal seams. *Journal of Natural Gas Science and Engineering, 56*, 299–314.

Lu, S., Zhang, Y., Sa, Z., Si, S., Shu, L., & Wang, L. (2019). Damage-induced permeability model of coal and its application to gas predrainage in combination of soft coal and hard coal. *Energy Science & Engineering, 7*, 1352–1367.

Lu, Y., Wang, L., Ge, Z., Zhou, Z., Deng, K., & Zuo, S. (2020). Fracture and pore structure dynamic evolution of coals during hydraulic fracturing. *Fuel, 259*, 116272.

Pan, J., Meng, Z., Hou, Q., Ju, Y., & Cao, Y. (2013). Coal strength and Young's modulus related to coal rank, compressional velocity and maceral composition. *Journal of Structural Geology, 54*, 129–135.

Puskarczyk, E., Krakowska-Madejska, P., Dohnalik, M., & Jelonek, I. (2022). Joint analysis using geomechanics, computed x-ray tomography and petrography based on coal samples from a carboniferous basin in Poland. *Bulletin of Engineering Geology and the Environment, 81*(3), 126.

Qiao, L., Hao, J., Liu, Z., Li, Q., & Deng, N. (2022). Influence of temperature on the transformation and self-control of energy during sandstone damage: Experimental and theoretical research. *International Journal of Mining Science and Technology, 32*, 761–777.

Qin, Y., Moore, T. A., Shen, J., Yang, Z., Shen, Y., & Wang, G. (2018). Resources and geology of coalbed methane in China: A review. *International Geology Review, 60*, 777–812.

Sampath, K. H. S. M., Perera, M. S. A., Elsworth, D., Ranjith, P. G., Matthai, S. K., & Rathnaweera, T. (2018). Experimental Investigation on the mechanical behavior of victorian brown coal under brine saturation. *Energy & Fuels, 32*, 5799–5811.

Song, H., Zhao, Y., Elsworth, D., Jiang, Y., & Wang, J. (2020). Anisotropy of acoustic emission in coal under the uniaxial loading condition. *Chaos, Solitons & Fractals, 130*, 109465.

Tan, P., Jin, Y., Hou, B., Han, K., Zhou, Y., & Meng, S. (2017). Experimental investigation on fracture initiation and non-planar propagation of hydraulic fractures in coal seams. *Petroleum Exploration and Development, 44*, 470–476.

Tao, Y., Li, Z., Cheng, Z., Zou, Q., Cao, J., & Huang, Y. (2021). Deformation and failure characteristics of composite coal mass. *Environmental Earth Sciences, 80*, 114.

Tarasov, B., & Potvin, Y. (2013). Universal criteria for rock brittleness estimation under triaxial compression. *International Journal of Rock Mechanics & Mining Sciences, 59*, 57–69.

Vishal, V., Ranjith, P. G., & Singh, T. N. (2015). An experimental investigation on behaviour of coal under fluid saturation, using acoustic emission. *Journal of Natural Gas Science and Engineering, 22*, 428–436.

Wang, W., Zhao, Y., Sun, Z., & Lu, C. (2021a). Effects of bedding planes on the fracture characteristics of coal under dynamic loading. *Engineering Fracture Mechanics, 250*, 107761.

Wang, Y., Feng, W. K., Hu, R. L., & Li, C. H. (2021b). Fracture evolution and energy characteristics during marble failure under triaxial fatigue cyclic and confining pressure unloading (FC-CPU) conditions. *Rock Mechanics and Rock Engineering, 54*, 799–818.

Wen, T., Tang, H., & Wang, Y. (2020). Brittleness evaluation based on the energy evolution throughout the failure process of rocks. *Journal of Petroleum Science and Engineering, 194*, 107361.

Wong, L. N. Y., Maruvanchery, V., & Liu, G. (2016). Water effects on rock strength and stiffness degradation. *Acta Geotechnica, 11*, 713–737.

Wu, C., Zhang, X., Wang, M., Zhou, L., & Jiang, W. (2018). Physical simulation study on the hydraulic fracture propagation of coalbed methane well. *Journal of Applied Geophysics, 150*, 244–253.

Wu, J., Zhang, S., Cao, H., Zheng, M., Qu, F., & Peng, C. (2020). Experimental investigation of crack dynamic evolution induced by pulsating hydraulic fracturing in coalbed methane reservoir1. *Journal of Natural Gas Science and Engineering, 75*, 103159.

Xie, H., Gao, M., Fu, C., Lu, Y., Yang, M., Hu, J., & Yang, B. (2021). Mechanical behavior of brittle-ductile transition in rocks at different depths. *Journal of China Coal Society., 46*, 701–715.

Xie, H., Li, L., Ju, Y., Peng, R., & Yang, Y. (2011). Energy analysis for damage and catastrophic failure of rocks. *Science China Technological Sciences, 54*, 199–209.

Xu, J., Zhai, C., Ranjith, P. G., Sang, S., Yu, X., Sun, Y., Cong, Y., Zheng, Y., & Tang, W. (2022). Mechanical responses of coals under the effects of cyclical liquid CO_2 during coalbed methane recovery process. *Fuel, 308*, 121890.

Xu, J., Zhai, C., Sang, S., Ranjith, P. G., Yu, X., Sun, Y., Cong, Y., Tang, W., & Zheng, Y. (2021). Brittleness evolution of different rank coals under the effects of cyclic liquid CO_2 during the coalbed methane recovery process. *Energy & Fuels, 35*, 17651–17662.

Yang, M., Yang, Z., Sun, B., Zhang, Z., Liu, H., & Zhao, J. (2020). A study on the flowability of gas displacing water in low-

permeability coal reservoir based on NMR technology. *Frontiers of Earth Science, 14*, 673–683.

Yao, Q., Wang, W., Li, X., Tang, C., Xu, Q., & Yu, L. (2021). Study of mechanical properties and acoustic emission characteristics of coal measures under water-rock interaction. *Journal of China University of Mining and Technology, 50*, 558–569.

Yin, D., Chen, S., Ge, Y., & Liu, R. (2021). Mechanical properties of rock–coal bi-material samples with different lithologies under uniaxial loading. *Journal of Materials Research and Technology, 10*, 322–338.

Zhang, L., Ren, T., Li, X., & Tan, L. (2021a). Acoustic emission, damage and cracking evolution of intact coal under compressive loads: Experimental and discrete element modelling. *Engineering Fracture Mechanics, 252*, 107690.

Zhang, P., Meng, Z., Zhang, K., & Jiang, S. (2020a). Impact of coal ranks and confining pressures on coal strength, permeability, and acoustic emission. *International Journal of Geomechanics, 20*, 04020135.

Zhang, S., Liu, H., Jin, Z., & Wu, C. (2021b). Multifractal analysis of pore structure in middle- and high-rank coal by mercury intrusion porosimetry and low-pressure N_2 adsorption. *Natural Resources Research, 30*, 4565–4584.

Zhang, X., Ranjith, P. G., Lu, Y., & Ranathunga, A. S. (2019a). Experimental investigation of the influence of CO_2 and water adsorption on mechanics of coal under confining pressure. *International Journal of Coal Geology, 209*, 117–129.

Zhang, X., Ranjith, P., Ranathunga, A., & Li, D. (2019b). Variation of mechanical properties of bituminous coal under CO_2 and H_2O saturation. *Journal of Natural Gas Science and Engineering, 61*, 158–168.

Zhang, Z., Deng, M., Bai, J., Yu, X., Wu, Q., & Jiang, L. (2020b). Strain energy evolution and conversion under triaxial unloading confining pressure tests due to gob-side entry retained. *International Journal of Rock Mechanics and Mining Sciences, 126*, 104184.

Zhao, C., Xing, J., Niu, J., & Ma, C. (2019a). Experimental study on crack propagation of precrack rock-like specimens under hydro-mechanical coupling. *Chinese Journal of Rock Mechanics and Engineering, 38*, 2823–2830.

Zhao, H., Wang, X., & Liu, Z. (2019b). Experimental investigation of hydraulic sand fracturing on fracture propagation under the influence of coal macrolithotypes in Hancheng block, China. *Journal of Petroleum Science and Engineering, 175*, 60–71.

Zhao, H., Wang, X., Liu, Z., Yan, Y., & Yang, H. (2018). Investigation on the hydraulic fracture propagation of multilayers-commingled fracturing in coal measures. *Journal of Petroleum Science and Engineering, 167*, 774–784.

Zhong, C., Zhang, Z., Ranjith, P. G., Lu, Y., & Choi, X. (2019). The role of pore water plays in coal under uniaxial cyclic loading. *Engineering Geology, 257*, 105125.

Zhong, J., Ge, Z., Lu, Y., Zhou, Z., & Zheng, J. (2020). New mechanical model of slotting-directional hydraulic fracturing and experimental study for coalbed methane development. *Natural Resources Research, 30*, 639–656.

Zhou, K., Dou, L., Song, S., Ma, X., & Chen, B. (2021). Experimental study on the mechanical behavior of coal samples during water saturation. *ACS Omega, 6*, 33822–33836.

Zhou, Z., Cai, X., Li, X., Cao, W., & Du, X. (2020). Dynamic Response and energy evolution of sandstone under coupled static-dynamic compression: Insights from experimental study into deep rock engineering applications. *Rock Mechanics and Rock Engineering, 53*, 1305–1331.

Zhu, W., & Tang, C. (2004). Micromechanical Model for Simulating the fracture process of rock. *Rock Mechanics and Rock Engineering, 37*, 25–56.

Zong, Y., Han, L., Meng, Q., & Wang, Y. (2020). Strength properties and evolution laws of cracked sandstone samples in re-loading tests. *International Journal of Mining Science and Technology, 30*, 251–258.